AIP Journal of Applied Physics

Efficient carrier relaxation and fast carrier recombination of N-polar InGaN/GaN light emitting diodes

Shih-Wei Feng, Po-Hsun Liao, Benjamin Leung, Jung Han, Fann-Wei Yang, and Hsiang-Chen Wang

Citation: Journal of Applied Physics **118**, 043104 (2015); doi: 10.1063/1.4927421
View online: http://dx.doi.org/10.1063/1.4927421
View Table of Contents: http://scitation.aip.org/content/aip/journal/jap/118/4?ver=pdfcov
Published by the AIP Publishing

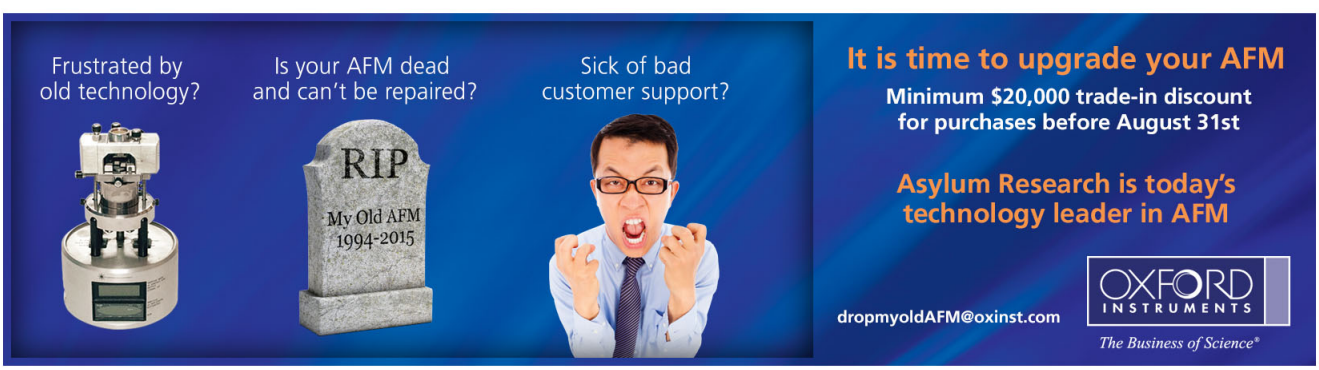

Efficient carrier relaxation and fast carrier recombination of *N*-polar InGaN/GaN light emitting diodes

Shih-Wei Feng,[1,a)] Po-Hsun Liao,[1] Benjamin Leung,[2] Jung Han,[2] Fann-Wei Yang,[3] and Hsiang-Chen Wang[4]
[1]*Department of Applied Physics, National University of Kaohsiung, No. 700, Kaohsiung University Rd., Nan Tzu Dist., 811 Kaohsiung, Taiwan*
[2]*Department of Electrical Engineering, Yale University, New Haven, Connecticut 06520, USA*
[3]*Department of Electronic Engineering, Southern Taiwan University of Science and Technology, Tainan, Taiwan*
[4]*Graduate Institute of Opto-Mechatronics and Advanced Institute of Manufacturing with High-Tech Innovations (AIM-HI), National Chung Cheng University, Chia-Yi, Taiwan*

(Received 17 March 2015; accepted 14 July 2015; published online 24 July 2015)

Based on quantum efficiency and time-resolved electroluminescence measurements, the effects of carrier localization and quantum-confined Stark effect (QCSE) on carrier transport and recombination dynamics of *Ga*- and *N*-polar InGaN/GaN light-emitting diodes (LEDs) are reported. The *N*-polar LED exhibits shorter *ns*-scale response, rising, delay, and recombination times than the *Ga*-polar one does. Stronger carrier localization and the combined effects of suppressed QCSE and electric field and lower potential barrier acting upon the forward bias in an *N*-polar LED provide the advantages of more efficient carrier relaxation and faster carrier recombination. By optimizing growth conditions to enhance the radiative recombination, the advantages of more efficient carrier relaxation and faster carrier recombination in a competitive performance *N*-polar LED can be realized for applications of high-speed flash LEDs. The research results provide important information for carrier transport and recombination dynamics of an *N*-polar InGaN/GaN LED. © *2015 AIP Publishing LLC*. [http://dx.doi.org/10.1063/1.4927421]

I. INTRODUCTION

III-Nitrides have become the key material for light-emitting diodes (LEDs), laser diodes, solar cells, and high electron mobility transistors (HEMTs).[1–6] The carrier localization effect caused by indium aggregation and the quantum-confined Stark effect (QCSE) resulting from a strain-induced piezoelectric field in those devices, generally grown along the *Ga*-polar *c*-axis [0001], were shown to determine the optical properties and device characteristics.[1–6] In spite of successful applications in optoelectronic devices, *Ga*-polar III-nitrides show some limitations. Because the optimal growth temperatures for the growth of GaN and InN are different, the low-quality, high-In InGaN exhibits a higher defect density and lower green light efficiency, i.e., the well-known "green gap."[7] Meanwhile, the reverse polarization field of III-nitrides along the *N*-polar *c*-axis [000$\bar{1}$] provides an alternative solution.[8–11] It is reported that the indium incorporation efficiency and photoluminescence (PL) peak intensity in *N*-polar InGaN/GaN multiple quantum wells (MQWs) grown by metal-organic chemical vapor deposition (MOCVD) and those in *N*-polar InGaN films grown by plasma-assisted molecular beam epitaxy (PAMBE) are higher than those in *Ga*-polar ones.[9,10] Also, due to the direction of the polarization field against the forward bias, a larger forward bias decreases the polarization field in *N*-polar InGaN/GaN MQWs, resulting in a flat-band and reduced QCSE.[11]

In addition, the properties of *N*-polar III-nitrides are different from those of *Ga*-polar ones; the direction of the polarization field in InGaN/GaN MQWs and AlGaN/GaN HEMTs, the incorporation of oxygen or carbon, mobility, and surface morphology are all different.[8,11–14] These different properties of the *N*-polar III-nitrides should affect the device characteristics. However, the effects of carrier localization and QCSE on carrier transport and recombination dynamics of *N*-polar InGaN/GaN MQW LEDs are not well studied.

This study reports the effects of carrier localization and QCSE on carrier transport and recombination dynamics of the *N*-polar InGaN/GaN MQW LED in comparison with those of the *Ga*-polar one by using current-voltage (*I-V*), electroluminescence (EL), quantum efficiency (QE), and time-resolved electroluminescence (TREL) measurements.

This paper is organized as follows: In Section II, sample structures and experimental procedures are described. In Section III, experimental results and discussions are reported. Finally, conclusions are drawn in Section IV.

II. SAMPLE STRUCTURES AND EXPERIMENTAL PROCEDURES

Ga- and *N*-polar GaN epilayers were grown on the *c*-axis of sapphires by a MOCVD reactor. For the *Ga*-polar GaN epilayer, the sapphire was thermally cleaned in H_2 at 1070 °C for 5 min prior to the deposition of 30 nm of low-temperature (LT) GaN buffer at 510 °C. *Ga*-polar undoped (2 μm thick) and Si-doped (2 μm thick) GaN films were grown at 1030 °C, 200 mbar, 2 slm NH_3, and 25 sccm

a)Author to whom correspondence should be addressed. Electronic mail: swfeng@nuk.edu.tw

trimethylgallium (TMGa). For the *N*-polar GaN epilayer, a 20 nm LT-GaN buffer was grown on nitridized sapphire at 600 °C in H_2, followed by *N*-polar undoped (2 μm thick) and Si-doped (2 μm thick) GaN films at 1030 °C, 100 mbar, 0.5 slm NH_3, and 13 sccm TMGa. The LED structures for the *Ga*- and *N*-polar LEDs, respectively, were regrown on the *Ga*- and *N*-polar GaN templates simultaneously in a MOCVD reactor. The LED structure consisted of 10 pairs of InGaN/GaN MQWs (3 nm QW, 12 nm barrier), AlGaN electron-blocking layer (EBL), and Mg-doped p-type GaN contact layer. The chip size of both *Ga*- and *N*-polar LEDs is $1 \times 1\,mm^2$.

I-V, EL spectrum, and output power were measured with a source meter (Keithley, 2614B), spectrometer (Ocean Optics, resolution 0.3 nm), and calibrated integrating sphere. For TREL measurement, a pulse generator (Tektronix, AFG3101C) was used to generate 2.0–5.0 V, 0.5 μs pulse width, and 1 kHz repetition rate voltage pulses to the LEDs. The rise/fall times of the voltage pulses are less than 5 ns. The light output was focused and detected by a photosensor module containing a metal package PMT and a high-voltage power supply circuit (Hamamatsu, H10721–210), operating directly on the surface of each LED. The rise time of the high-sensitivity photosensor module is 0.57 ns. The transit EL signals were recorded by a digital oscilloscope (Agilent, DSO 6052 A) with a 500 MHz bandwidth. The condition of impedance matching can be attained with a variable resistor by mining the reflected current pulse monitored by an oscilloscope. All the measurements were carried out at room temperature. The overall resolution of TREL system can be less than 2 ns.

III. EXPERIMENTAL RESULTS AND DISCUSSIONS

A. EL image, EL spectra, and energy band diagrams

Figs. 1(a) and 1(b) show the EL spectra for *Ga*- and *N*-polar LEDs, respectively. For the *N*-polar LED, a broader bandwidth and an apparent low energy shoulder imply larger fluctuations of indium composition and quantum well thickness and a stronger carrier localization. Insets of Figs. 1(a) and 1(b) show EL images of the *Ga*- and *N*-polar LEDs operated under 3.0 V continuous-wave (CW) applied voltage, respectively. The top and bottom electrodes correspond to *p*- and *n*-contact pads, respectively. The brighter EL image of the *Ga*-polar LED than that of the *N*-polar LED shows better performance in the *Ga*-polar LED. In addition, Fig. 1(c) shows EL peak position as a function of CW applied voltage for the two samples. Due to the different directions of the polarization field in the QWs, the electric field in *Ga*-polar MQWs increases with increasing forward bias up to 2.5 V, while it decreases in *N*-polar MQWs.[15] With a larger forward bias above 2.5 V, carrier injection into *Ga*-polar MQWs results in a carrier screening effect and the electric field becoming smaller, while the electric field decreases even more in *N*-polar MQWs. A significantly blue-shifted emission wavelength of EL peak position at a slightly higher applied voltage for *N*-polar LEDs could be due to the band filling effect of the localized states, a reduced QCSE, and a larger variation of QCSE with a forward bias. Although a

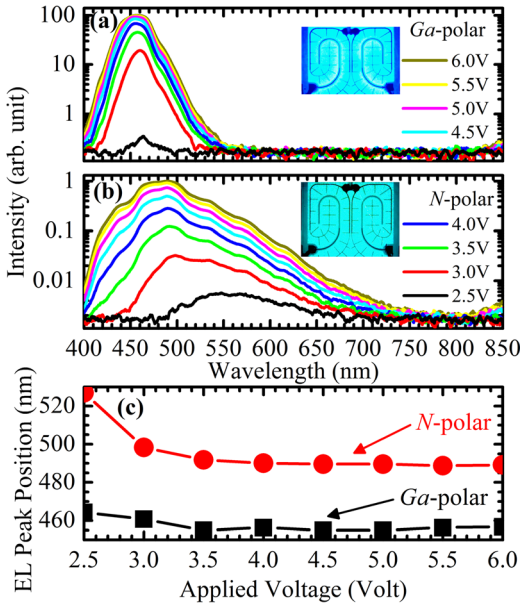

FIG. 1. EL spectra of the (a) *Ga*- and (b) *N*-polar LEDs at room temperature with 2.5–6.0 V CW applied voltages. (c) EL peak position as a function of CW applied voltage for the two types of LED. Insets of (a) and (b) show EL images of the *Ga*- and *N*-polar LEDs operated under 3.0 V CW applied voltage, respectively. The top and bottom electrodes correspond to *p*- and *n*-contact pads, respectively.

reduced QCSE leads to a flat band condition, both a higher indium incorporation and a stronger carrier localization in the *N*-polar LED lead to more fluctuated and lower effective potential levels in MQWs. Hence, an emission wavelength of EL peak position in the *N*-polar LED is longer than that in the *Ga*-polar LED for each applied voltage. On the other hand, with a larger forward bias, a smaller electric field also leads to a slightly blue-shifted emission wavelength of EL peak position for the *Ga*-polar LED.

As shown in Fig. 2, the energy band diagrams of *Ga*- and *N*-polar InGaN/GaN MQWs were calculated using a self-consistent Schrödinger-Poisson equation that considers

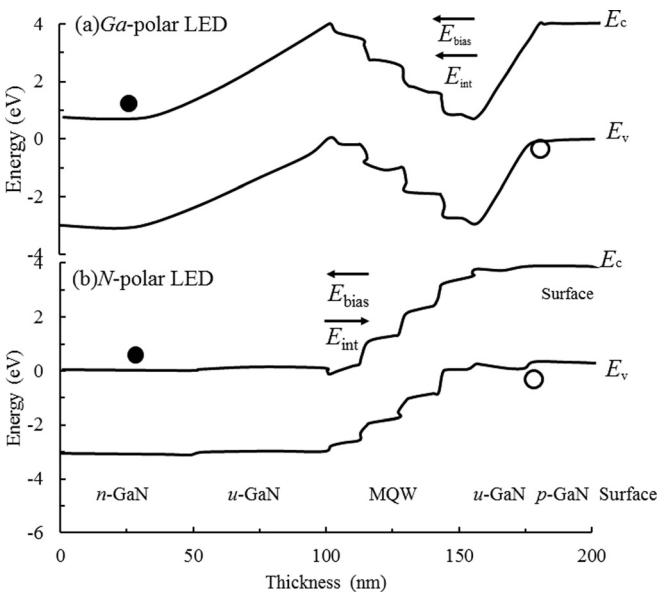

FIG. 2. Energy band diagrams of *Ga*- and *N*-polar LEDs.[11]

spontaneous and piezoelectric polarization.[11] In Fig. 2(a), polarization charges in *Ga*-polar MQWs generate a potential barrier for electron and hole injection, which decreases carrier injection efficiency. A forward bias increases the field and decreases the overlap of electron and hole wavefunctions. In Fig. 2(b), the potential barrier against the injection in an *N*-polar LED is suppressed such that carrier injection efficiency would be higher. Due to the reverse polarization in an *N*-polar LED, a larger forward bias assists the field in MQWs to approach flat-band conditions leading to less QCSE and an increasing overlap of electron and hole wave functions.

B. *I-V* characteristics and external quantum efficiency (EQE)

Fig. 3(a) shows the *I-V* characteristics of the two samples. A slightly larger threshold and a smaller slope of current under forward bias, and a larger leakage current under reverse bias of the *N*-polar LED suggest unoptimized ohmic contacts of and poorer device quality with the *N*-polar LED than that of and with the *Ga*-polar LED. In addition, Fig. 3(b) shows the output power and EQE of the two samples as functions of applied voltage. The higher output power and higher EQE of the *Ga*-polar LED demonstrate a better device performance.

C. TREL measurement

In order to understand the carrier transport and recombination dynamics of *Ga*- and *N*-polar LEDs, TREL measurements were conducted. Figs. 4(a) and 4(b) show the TREL transit profiles of *Ga*- and *N*-polar LEDs, respectively. The rising part of the *N*-polar LED rises more steeply and the decay part decays faster than those of the *Ga*-polar LED. These shorter response time and shorter recombination time of the *N*-polar LED imply a better carrier injection efficiency and a faster carrier recombination, respectively.

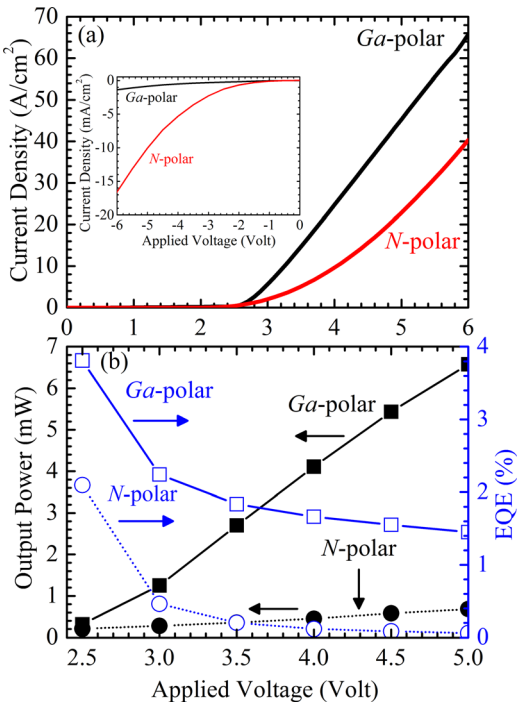

FIG. 3. (a) Current density (*I*) and (b) output power (left coordinate) and EQE (right coordinate) as functions of applied voltage (*V*) for the two types of LED. Inset in (a) shows the *I-V* characteristics under reverse bias.

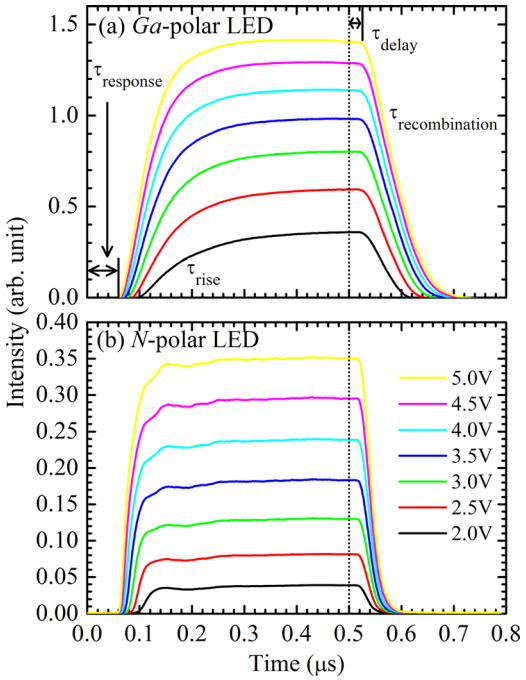

FIG. 4. TREL transit profiles with 2.0–5.0 V, 0.5 μs pulse width, and 1 kHz repetition rate applied pulse voltages for the (a) *Ga*- and (b) *N*-polar LEDs, with the vertical dotted line indicating the pulse voltage switching off. Response ($\tau_{response}$), rise (τ_{rise}), delay (τ_{delay}), and recombination ($\tau_{recombination}$) times are shown in (a).

As shown in Fig. 5, the response time ($\tau_{response}$) can be determined by the time delay between addressing the device with a short voltage pulse and the first appearance of EL. Because a larger forward bias enhances the ability of the hole and electron leading fronts to meet faster and more easily, a shorter response time is observed. Response time, $\tau_{response}$, can be described as

$$\tau_{response} = \tau_{injection} + \tau_{transport} + \tau_{relaxation} + \tau'_{recombination},$$

where $\tau_{injection}$, $\tau_{transport}$, $\tau_{relaxation}$, and $\tau'_{recombinaiton}$ are the carrier injection time to the ohmic contact, carrier transport time from the ohmic contact to the active region, carrier relaxation time from the active region to the MQWs, and carrier recombination time in the energy states, respectively. With the same contact material for the two samples, $\tau_{injection}$ is assumed to be the same. Also, due to the smaller mobility of *N*-polar GaN, $\tau_{transport}$ of the *N*-polar LED should be longer than that of the *Ga*-polar LED. Meanwhile, it is reported that polarization charges in *Ga*-polar MQWs generate a potential barrier before carrier relaxation into the MQWs, while the reverse polarization field suppresses the potential barrier upon a forward bias in *N*-polar MQWs.[11] The carrier relaxation efficiency of the *N*-polar LED is better than that of the *Ga*-polar LED, so $\tau_{relaxation}$ of the *N*-polar LED should be shorter than that of the *Ga*-polar LED. In the *N*-polar

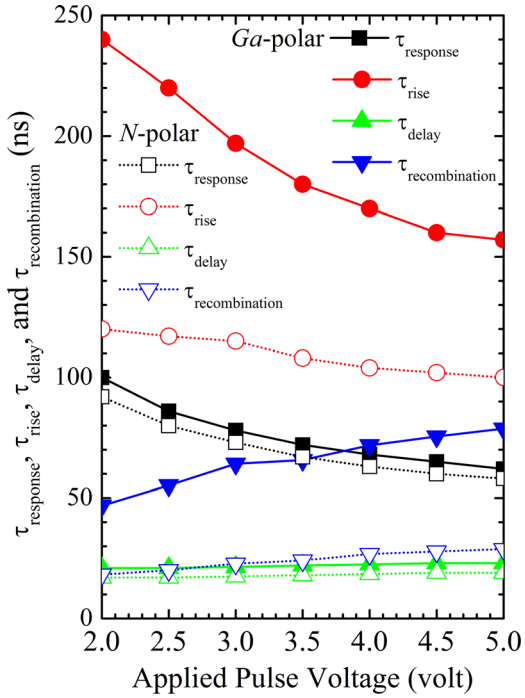

FIG. 5. Response ($\tau_{response}$), rise (τ_{rise}), delay (τ_{delay}), and recombination ($\tau_{recombination}$) times as functions of applied pulse voltage for the two types of LED.

LED, a forward bias decreases the QCSE and increases the overlap of electron and hole wave-function. The $\tau'_{recombinaiton}$ of the *N*-polar LED is expected to be shorter, as shown later. Hence, the shorter $\tau_{response}$ of the *N*-polar LED should be due to a shorter $\tau_{relaxation}$ and a shorter $\tau'_{recombinaiton}$. This suggests that stronger carrier localization helps carrier relaxation into MQWs and carrier recombination in the energy states, as do the combined effects of the suppressed QCSE and electric field and the lower potential barrier acting upon the forward bias in an *N*-polar LED.

After the appearance of EL, the transit EL profile steeply increases in reaching the maximum intensity. The rising time (τ_{rise}), defined by the intercept of the tangents,[16] as a function of applied pulse voltage is shown in Fig. 5. τ_{rise} of the *N*-polar LED is shorter than that of the *Ga*-polar LED for each applied voltage. With the combined effects of a stronger carrier localization, plus a weaker QCSE and electric field and lower potential barrier upon the forward bias in the *N*-polar LED, a better carrier relaxation efficiency leads to a steeper rise of the transit EL profile. Hence, a shorter τ_{rise} is observed. Meanwhile, with a weaker carrier localization, a stronger QCSE, and a potential barrier in the *Ga*-polar LED, the poor carrier relaxation efficiency leads to a slower rise of the transit EL profile. Also, with an increasing applied pulse voltage, τ_{rise} of the *N*-polar LED slightly decreases, while those of the *Ga*-polar LED decrease more. For the *N*-polar LED, the smaller QCSE largely does not affect the potential distribution upon a larger forward bias and the overlap integral of electron and hole wavefunctions. Hence, τ_{rise} of the *N*-polar LED depends only slightly on the forward bias. In the contrast, the larger QCSE and larger variations of QCSE and potential distribution upon a forward bias in the *Ga*-polar LED have a great effect on the overlap integral of electron and hole wavefunctions.

In addition, when the voltage pulse is switched off (indicated with the vertical dotted line in Figs. 4(a) and 4(b)), transit EL profiles of the *Ga*-polar LED show longer delays in reaching both the maximum intensity of transit EL and the subsequent decay. As shown in Fig. 5, due to the combined effects of the weaker carrier localization, stronger QCSE, and the potential barrier, the poorer relaxation efficiency of the *Ga*-polar LED needs more time to reach the maximum intensity of transit EL. Hence, shorter *ns*-scale $\tau_{response}$, τ_{rise}, and τ_{delay} in the *N*-polar LED demonstrate that stronger carrier localization, plus reduced QCSE, and lower potential barrier acting upon the forward bias, provide the advantage of more efficient carrier relaxation.

The recombination time ($\tau_{recombination}$) can be determined by fitting the TREL decay profile with a single exponential. Fig. 5 shows $\tau_{recombination}$ as a function of applied pulse voltage for the two samples. With a larger applied pulse voltage, $\tau_{recombination}$ of the *N*-polar LED slightly increases, while that of the *Ga*-polar LED increases more. This also could be due to the larger QCSE and larger variations of QCSE and potential distribution upon a larger forward bias for the *Ga*-polar LED. Also, $\tau_{recombination}$ of the *N*-polar LED is shorter than that of the *Ga*-polar LED for each applied pulse voltage. The shorter $\tau_{recombination}$ of the *N*-polar LED implies that stronger carrier localization, reduced QCSE, and an increasing overlap of electron and hole wave functions are beneficial for carrier recombination. The recombination time ($1/\tau_{recombination} = 1/\tau_r + 1/\tau_{nr}$) includes radiative ($\tau_r$) and nonradiative ($\tau_{nr}$) recombination times. It is noted that the obtained $\tau_{recombinaiton}$ is the temporal decay of the EL at the end of the applied voltage pulse, while $\tau'_{recombinaiton}$ in $\tau_{response}$ is the carrier recombination of only a few carriers in the leading fronts of hole and electron pulses. With many carriers relaxed into the MQWs at the end of the applied voltage pulse, carrier-carrier scattering would change the recombination dynamics. $\tau_{recombinaiton}$ may not be equal to $\tau'_{recombinaiton}$. By optimizing growth conditions to enhance the radiative recombination, the advantages of more efficient carrier relaxation and the faster carrier recombination of the *N*-polar LED can be realized for high-speed flash LED application. Several approaches have been proposed to improve the characteristics of the *N*-polar GaN: a high temperature nitridation step prior to the deposition of the GaN nucleation layer, a lower pressure and a reduced NH_3 flow, a low-temperature GaN buffer, and growth on misorientated substrates.[8,10,17] The temporal decay of the EL at the end of the applied voltage pulse indicates the depletion of the carrier reservoir established during the preceding on-phase.

IV. CONCLUSIONS

In summary, this paper reports the effects of carrier localization and QCSE on carrier transport and recombination dynamics of *Ga*- and *N*-polar InGaN/GaN LEDs. Stronger carrier localization, plus reduced QCSE and electric field and lower potential barrier acting upon the forward bias in the *N*-polar LED, present more efficient carrier relaxation and

faster carrier recombination. By optimizing growth conditions to enhance the radiative recombination, the advantages of more efficient carrier relaxation and faster carrier recombination in the *N*-polar LED can be realized for the applications of high-speed flash LEDs. The research results provide important information for carrier transport and recombination dynamics of an *N*-polar InGaN/GaN LED.

ACKNOWLEDGMENTS

This research was supported by the Ministry of Science and Technology, Taiwan, under Grant Nos. NSC 99-2112-M-390-002-MY3, NSC 102-2112-M-390-001, and MOST 103-2112-M-390-002.

[1]S. Nakamura and G. Fasol, *The Blue Laser Diode* (Springer, Berlin, 1997).
[2]E. Fred Schubert, *Light-Emitting Diodes*, 2nd ed. (Cambridge University Press, Cambridge, 2006).
[3]Y. Narukawa, Y. Kawakami, S. Fujita, S. Fujita, and S. Nakamura, Phys. Rev. B **55**, R1938 (1997).
[4]S. W. Feng, C. M. Lai, C. H. Chen, W. C. Sun, and L. W. Tu, J. Appl. Phys. **108**, 93118 (2010).
[5]S. W. Feng, Y. Y. Chen, C. M. Lai, L. W. Tu, and J. Han, J. Appl. Phys. **114**, 233103 (2013).
[6]S. Rajan, H. Xing, S. DenBaars, U. K. Mishra, and D. Jena, Appl. Phys. Lett. **84**, 1591 (2004).
[7]C. Wetzel and T. Detchprohm, Compd. Semicond. **15**, 21 (2009).
[8]Q. Sun, Y. S. Cho, I. H. Lee, J. Han, B. H. Kong, and H. K. Cho, Appl. Phys. Lett. **93**, 131912 (2008).
[9]D. N. Nath, E. Gür, S. A. Ringel, and S. Rajan, Appl. Phys. Lett. **97**, 71903 (2010).
[10]S. Keller, N. A. Fichtenbaum, M. Furukawa, J. S. Speck, S. P. DenBaars, and U. K. Mishra, Appl. Phys. Lett. **90**, 191908 (2007).
[11]F. Akyol, D. N. Nath, E. Gür, P. S. Park, and S. Rajan, Jpn. J. Appl. Phys. Part 1 **50**, 052101 (2011).
[12]S. Rajan, A. Chini, M. H. Wong, J. S. Speck, and U. K. Mishra, J. Appl. Phys. **102**, 044501 (2007).
[13]N. A. Fichtenbaum, T. E. Mates, S. Keller, S. P. DenBaars, and U. K. Mishra, J. Cryst. Growth **310**, 1124 (2008).
[14]A. Y. Polyakov, N. B. Smirnov, A. V. Govorkov, Q. Sun, Y. Zhang, Y. S. Cho, I. H. Lee, and J. Han, Mater. Sci. Eng., B **166**, 83 (2010).
[15]F. Akyol, Master thesis, The Ohio State University, 2011.
[16]S. Barth, P. Müller, H. Riel, P. F. Seidler, W. Rieß, H. Vestweber, and H. Bässler, J. Appl. Phys. **89**, 3711 (2001).
[17]S. Keller, N. A. Fichtenbaum, F. Wu, D. Brown, A. Rosales, S. P. DenBaars, J. S. Speck, and U. K. Mishra, J. Appl. Phys. **102**, 083546 (2007).